Nanoscale

Accepted Manuscript

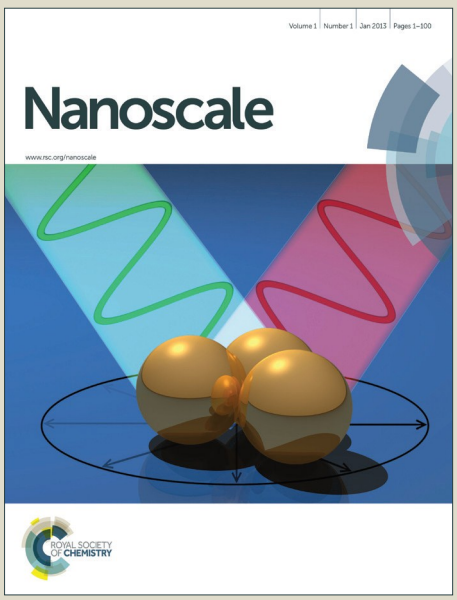

ROYAL SOCIETY OF CHEMISTRY

www.rsc.org/nanoscale

Cite this: DOI: 10.1039/c0xx00000x

www.rsc.org/xxxxxx

Full Paper

Large Scale Atomistic Simulation of Single-layer Graphene Growth on Ni(111) Surface: Molecular Dynamics Simulation Based on A New Generation of Carbon-Metal Potential

Ziwei Xu,[a] Tianying Yan,[b] Guiwu Liu,[a] Guanjun Qiao[a] and Feng Ding *[c]

Received (in XXX, XXX) Xth XXXXXXXXX 20XX, Accepted Xth XXXXXXXXX 20XX
DOI: 10.1039/b000000x

To explore the mechanism of graphene chemical vapor deposition (CVD) growth on catalyst surface, molecular dynamics (MD) simulation of the carbon atom self-assembly on Ni(111) surface based on a well-designed empirical reactive bond order potential was performed. We simulated a single layer graphene with recorded size (up to 300 atoms per super cell) and reasonable good quality by MD trajectories up to 15 ns. Detailed process of graphene CVD growth, such as carbon atom dissolution and precipitation, formation of carbon chains of various lengths, polygons and small graphene domains were observed during the initial process of the MD simulation. The atomistic processes of typical defect healing, such as the transformation from pentagon into hexagon and from pentagon-heptagon pair (5|7) to two adjacent hexagons (6|6), were revealed as well. The study also showed that higher temperature and longer annealing time are essential to form high quality graphene layers, which are in agreement with experimental reports and previous theoretical results.

1. Introduction

Motivated by the extraordinary thermal, electronic, optical, and mechanical properties of graphene, synthesis of high quality graphene in large area, large scale with cheap price is highly desired for many applications. Extensive efforts have been dedicated to develop the methods for graphene production to replace mechanical cleavage method, which is firstly proposed in 2004.[1] Among the numerous known methods of graphene synthesis,[2] the sublimation of SiC single crystal [3] and the chemcial vapor deposition (CVD) growth on a transition metal surface are two suitable methods for high quality graphene synthesis. Comparing to the sublimation of SiC, the CVD method has the advantages of relatively low experimental temperature and much more tunable experimental parameters, including temperature, type, quality and, the facet of the transition metal substrate, types and partial pressure of the feedstock and/or various carrier gases, etc. Experimentally, it was discovered that varying each of the factor will greatly alter the quality of the synthesized graphene, and thus the optimum experimental design is very difficult without deep insight into the mechanism of graphene CVD growth.

Many transition metals (e.g., Au,[4] Cu,[5, 6] Ni,[7] Co,[8, 9] Fe,[10] Pt,[11] Pd,[12] Ru,[13, 14] Rh,[15] Ir,[13] etc.) or their alloys (e.g., Ni-Mo,[16] Cu-Ni,[17, 18], etc.) are found to be capable to catalyze the graphene in CVD growth. Among them, Cu and Ni, or their alloys are two the most explored transition metals, probably due to their high availability and high efficiency. The mechanisms of graphene CVD growth on Cu and Ni are very different, due to the very different carbon solubility in them. Because of the extremely low carbon solubility, the graphene growth on Cu is a self-limited process, in which the carbon is supplied by the diffusion of carbon feedstock decomposed on the exposed Cu surface around.[19] Because feedstock cannot access the graphene covered Cu surface, there is no sufficient carbon supply beneath the first graphene layer, and only single layer graphene can be formed on the Cu surface at most.[20] On the other hand, the formation of the graphene on Ni surface is mostly attributed to the precipitation of the dissolved carbon atoms in the bulk. Thus, the number of synthesized graphene layers can be controlled by tuning the carbon solubility and precipitation.[7]

Besides the extensive experimental studies on the mechanism of graphene CVD growth, great theoretical efforts have also been dedicated to understand the atomistic process of graphene nucleation and growth on the transitional metal surface. Chen *et al.* showed that carbon dimer formation is energetically preferable than the monomers on Cu (111) surface, but carbon monomer is more preferred on the Ir(111) and Ru(0,0,0,1) surfaces through *ab initio* calculations.[21] By systematically investigating the formation of carbon clusters on many catalyst surface, Gao *et al*. showed that chain is the most preferred structure for small carbon clusters (N_c <= 10) on Ni (111) surface, and a nucleus of graphene is normally accompanied by topological defects, such as pentagons.[22-25] Wu *et al.* have explored the decomposition of the mostly used carbon feedstock CH_4 both on Cu surface and in air, and found that CH_i (i =1, 2, 3) radicals may play an important role in graphene CVD growth.[26, 27] Zhang *et al*. demonstrated the significant role of both the graphene wall-catalyst interaction and the graphene edge-catalyst interaction in the orientation of the domain during the epitaxial growth of the graphene.[28, 29] Wang *et al.* investigated the

formation and healing mechanisms of the vacancies and defects in the graphene.[30, 31] In addition, the structure and the stability of the graphene edges during the CVD growth have also been

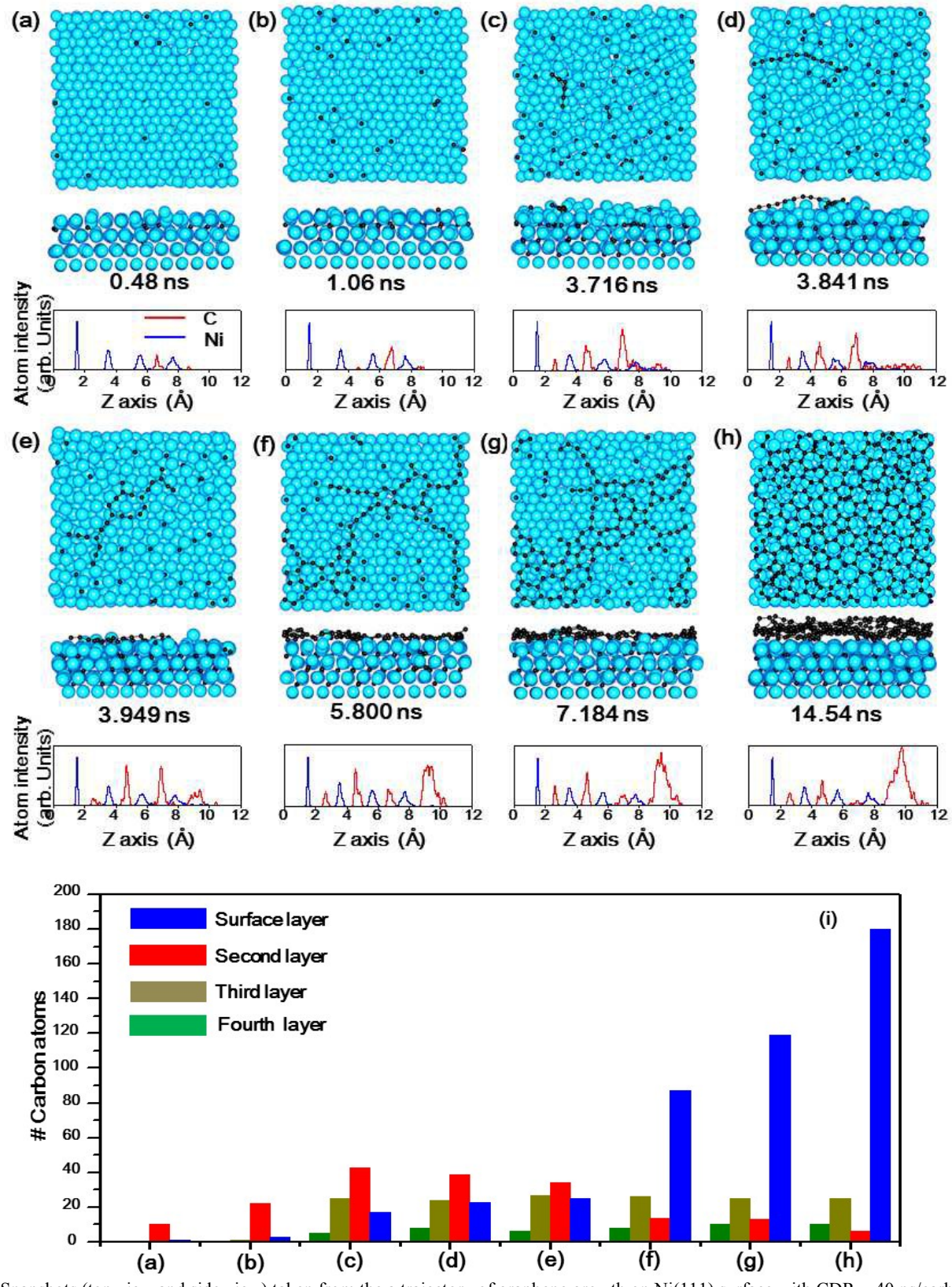

Fig. 1 Snapshots (top view and side view) taken from the a trajectory of graphene growth on Ni(111) surface with CDR = 40 ps/carbon at the temperature of 1300 K. (a), (b), (c), until (h) present the simulated details of the graphene growth at different MD simulation times. In each panel, the top view, side view, and the spectrum of atomic concentration are displayed, respectively. (i) The numbers of carbon atoms on the surface and between layers of the Ni substrate as those in (a), (b), until (h).

Cite this: DOI: 10.1039/c0xx00000x

www.rsc.org/xxxxxx

extensively investigated.[32-34]

Besides the aforementioned theoretical investigations based on the *ab initio* calculations, Monte Carlo (MC) and molecular dynamics (MD) simulations own the advantage of the temperature effect, so that kinetics and dynamics can be naturally considered. Previous atomic simulations can be classified into two categories, i.e., those based on a classical potential energy surface (PES), and those based on the semi-empirical tight binding (TB) model or density functional theory (DFT).[35] Based on the reactive force filed (ReaxFF), both Meng *et al.*[36] and Neyts *et al*.[37] performed the growth of the single layer graphene on the nickel substrate. The difference between the above two studies is that the former one focused the aggregation process with a given number of the carbon atoms, while the later one studied the growing process of the graphene with the gradual addition of the carbon atom to nickel surface. Using LAMMPS code, Rasuli et al. performed a classical MD of graphene growth on Ni (100) facet in which the C-Ni inteaction is described by the Lenard-Jones potential.[38] Based on the TB model of the carbon – nickel system, Amara *et al.* used the grand canonical Monte Carlo (GCMC) method to simulate the formation of of the carbon structure on nickel surface,[39, 40] including the atomic details on the defect healing with the assistance of nickel particles.[41] Morokuma *et al*. studied subsurface nucleation of the graphene precursors on the Ni(111) step edge,[42] and explored the template effect of the graphene flake to the growth of graphene on Ni(111) surface[43, 44] based on the quantum mechanical molecular dynamics (QM/MD). In addition, by using the *ab initio* MD (AIMD) based on the density functional theory (DFT), Özcelick *et al.* investigated the growing process of single layer graphene with and without substrates (Boron-Nitride substrate and the Ni substrate).[45]

These atomistic simulations, however, suffer the drawbacks of either the small size of the simulated graphene/metal system (most simulated super-cells has only ~ 100 or less C atoms) and/or very short affordable simulation time (~ 0.1 ns for most QM/MD and AIMD simulations). Hence, large scale graphene domains with reasonable high quality were obtained in these simulations. Limited by the small size scale (~ 260 Ni, ~150 C) and time scale (~100 ps) as well as the less accurate of the potential energy surface,[36-38] the full pictures on the carbon dissolution, surface precipitation and the crystallinity variation of each layer along the direction normal to the surface have not been displayed in those previous works. The atomic details on the formation of the carbon network and the defects healings have also not been presented elaborately though minor discussions were spotted. Besides, temperature effects and carbon deposition rates (CDR) during the graphene growth cannot be fully explored due to the intensive load on computation with the QM-based methods. In this study, we use the classical MD method to simulate the graphene CVD growth on the Ni(111) surface with a large super-cell of 2.556 x 2.6562 nm^2, in which a fully covered graphene domain of ~ 300 carbon atoms are simulated. To our best knowledge, the current simulation represents the largest one ever reported by atomic simulations. Similar to the previous work[37], a sequential addition of the carbon atoms is applied during the simulation, but with a much slower CDR of every atom per 10 - 40 ps. Through the simulation of larger MD time scale up to 15 ns, the single layer graphene with reasonable good quality was obtained under the optimized temperature of 1300 K. Further investigation showed that the lower temperature and faster carbon deposition reduces the quality of the simulated graphene, and the precipitation of C atoms from the subsurface also plays an important role in the constant temperature graphene CVD growth on the Ni(111) surface.

2. COMPUTATIONAL METHODS AND DETAILS

Classical MD simulation was performed to study the formation of graphene on Ni(111) surface. The carefully designed PES used in the MD is same as that used in the simulation of growth of carbon nanotubes.[46] Such a PES is based on a modified second generation of the reactive empirical bond order (REBO2) potential[47] of carbon-carbon and carbon-Ni interactions,[46] and the many-body tight-binding (TB) Metal-Metal interaction[48] and was fitted by a large basis of carbon-metal interactions.[46] Motivated by the pioneer works[49, 50], particularly by the work of Martinez-Limia et al.,[51] the new C-M interaction takes the style of Tersoff-Brenner potential with the screening effect of C-C interaction considered under various environments. The 26 parameters in the potential are fitted based on a large set of data basis calculated by the density functional theory (DFT). Besides, the angle dependent graphene edge-catalyst interaction, not included in any of previous PESs but very important for the formation of the graphitic caps,[23] is also considered in our PES. Based on several benchmarks, the tested results of the PES with other typical PESs validated the improvements of the accuracy of our PES [see the details in the ESI of reference[46]]. With such new PES, we are able to perform a simulation with larger size scale (up to 1000 atoms) and time scale (up to 10-100ns). A four-layer Ni (111) slab with the atoms of the bottom layer fixed is used as the catalyst substrate. Periodic boundary condition with a rectangle super-cell of of 2.556 × 2.6562 nm^2 is applied to mimic the semi-infinite surface. For the simplicity of the simulation, the decomposition and deposition of the hydrocarbon molecules were simplified as the sequentially addition of the single carbon atom on to the initially naked Ni(111) surface. In order to study the effects of the CDR to the graphene formation, the time interval between carbon atom addition is set to 20 ps/carbon and 40 ps/carbon, respectively. Similarly, three temperatures (900 K, 1100 K and 1300 K) are explored to investigate the effects of temperature on the graphene CVD growth. During the MD simulation, Newton's equation of motion is integrated by using velocity Verlet algorithm, and the Berendsen thermostat[52] is adopted to maintain the constant temperature of the system.

3. Results AND DISCUSSION

3.1 Atomic details of the graphene growth

Figure 1 shows the atomistic details of the graphene growth on the Ni(111) surface. The CDR and the temperature for this trajectory are 40 ps/carbon and 1300 K, respectively. Initially, carbon atom deposition on the nickel surface leads to the dissolution of them into the subsurface of the nickel layers (Figure 1 a, b, c and i). It is found that the solution of the carbon atoms greatly altered the structure of the Ni substrate and surface melting-like behavior, and the disordering of the Ni(111) crystal lattice on the topmost layer, can be clearly seen. As displayed in the bottom of figure 1a, the four blue peaks in the spectrum of the concentration of atoms correspond to the four Ni layers, respectively. The first sharp blue peak near 1.5Å corresponds to the bottom layer, the atoms of which are constrained during the simulation. The following three blue peaks from left to right correspond to the third, second and the top layers of the nickel substrate. The red peak around 6.5Å correspond the dissolved carbon atoms located in the subsurface between the top and the second nickel layers. As a consequence of the surface-melting of the nickel substrate induced by the dissolved carbon atoms, the peak of the first nickel layer becomes broader and broader during the deposition of carbon atoms in the initial stage of graphene growth (Figure 1 a→b→c→d). The high temperature of atomic simulation, 1300 K, enables the carbon atom diffusing deeply into the nickel substrate gradually as shown in Figure 1b-d.

With more and more carbon atoms dissolved into the Ni bulk, the nickel substrate reaches saturation. Therefore, the deposited carbon atoms tend to aggregate on the nickel topmost surface to form a graphene layer via the following steps:

i) Firstly, carbon dimers, trimmers, and carbon chains are formed (Figure 1c-d);

ii) Latterly, longer carbon chains with the "Y" junctions can be seen, and at the central atom of each "Y" junction becomes sp^2 hybridized (Figure 1e);

iii) Then, a carbon polygon can be seen near the sp^2 hybridized carbon atom of the "Y" junction;

iv) The initially nucleated polygon serves as a center of nucleation, and more and more polygons are formed around it as a polygon cluster or a graphene nucleus as shown in Figure 1f-g;

v)By keep forming new polygons, the nucleus grows larger and large until the full surface was covered by graphene (Figure 1h).

It should be noted that the nucleation of the graphene on their nickel surface is not a simple “2D” mechanism but a more complicated “3D” problem. Previous simulation show that the graphene nucleates from the amorphous nickel carbides accompanied a strong degradation of the nickel surface[53, 54] and its kinetics depends largely on the carbon density of the subsurface. In our simulation, however, due to the sequential addition of the carbon atoms, the graphene nucleation stems from both the diffusion of the continually deposited carbon atoms and the precipitated carbon atoms from the subsurface.

Before polygon nucleation, the concentration peaks of the top and second nickel layer become broader and broader, indicating the lattice disordering of the top and second nickel layers induced by the carbon dissolution. The overlap of the red and blue peaks near 5.5 Å and 7.5 Å in Figure 1d demonstrates that some dissolved carbon atoms can be mixed with the top and second nickel layers. Meanwhile, the broadened peaks of the top and second Ni layers become sharp again when the carbon polygons are formed (Figure 1e). Simultaneously, the peak of the carbon atoms on the nickel substrate surface becomes larger and larger, accompanying with the formation of carbon chains, polygons, and polygon clusters or small graphene domains on the topmost layer. This implies that the formation of a graphene layer above the Ni surface could restore the crystallinity of the catalyst substrate during graphene CVD growth. To prove the evolution of nickel surface during the carbon dissolution and precipitation, we calculate the lindemann index (Figure S1) as function of the MD time, a simple measure monitoring the disorder of the atoms. The sharp signal of the lindemann index appears at the vicinity of 3.8 ns indicating the disordered lattice of the nickel surface, which agrees well with the Figure 1 (d). Also, the signal decline of the lindemann index after 3.9 ns proves that the crystallinity of the nickel surface starts to restore due to the formation of the graphene.

It is interesting that the peaks of the subsurface carbon atoms becomes very high before the nucleation of the polygons (Figure 1c-e). On the other hand, when long C chains and polygons are formed on the catalyst surface, the peak of the subsurface catbon atoms was greatly reduced (figure 1f, g), and only ~ 1/3 of the carbon atoms remain in the subsurface. Furthermore, the carbon solubility in the subsurface was even lowered during the enlargement of the graphene domain on the catalyst surface (Figure 1h). The huge reduction of the carbon solubility implies the change of chemical potential of the dissolved carbon atoms during graphene growth. According to the classical crystal growth theory, initiation of a crystal nucleation requires to overcome a barrier of nucleation, which is a function of the chemical potential.[22] The large carbon solubility in the subsurface implies a large chemical potential, i.e.,

$$\mu \sim k\mathrm{T}\ln c, \qquad (1)$$

where k is the Boltzmann constant, T is the temperature and c is the concentration of the dissolved C atoms in the subsurface. Such a high chemical potential reduces the 2D nucleation barrier of the graphene on the Ni surface, and enables the nucleation of longer carbon chains, polygons, and polygon clusters or small graphene domains. Once the polygon cluster or small graphene domains are formed, these active carbon atoms in the subsurface can be quickly precipitated to the surface of the Ni and then be attached to the polygon cluster or small graphene domains. The precipitation of the dissolved carbon atoms reduces the chemical potential and increases the barrier of graphene nucleation. The increased nucleation barrier disables the nucleation of many graphene domains nearby the first one, and consequently reduces the nucleation density. As evidenced in our simulation, there are only two linked graphene nuclei that are formed on the simulated super-cell.

3.2 Defects healing during the pure MD

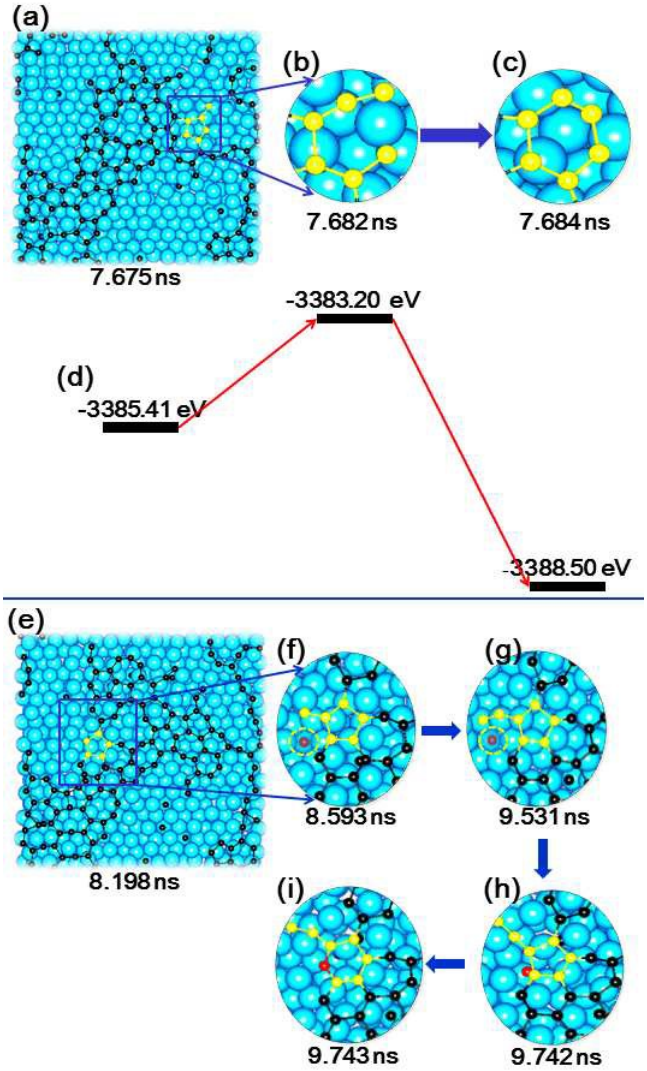

Fig. 2 Two different routes of the pentagon healing. (a)→(c) A carbon atom is attached to the pentagon and then the pentagon-dangling atom formation is transformed into a hexagon by the rotation of a carbon-carbon bond. (d) The potential energies of configurations (a), (b) and (c). (e)→(i) A pentagon (highlighted in yellow) is attached by a carbon chain and is transformed into a hexagon by the incorporation of the carbon atom (highlighted in red) from the subsurface of the nickel substrate. The dashed circles in (e) and (f) indicate the position of the nickel atom on the top of the carbon atom, which is removed for sake of clear display.

As shown in figure 1, the defects formation, such as pentagons, heptagons, octagons, etc., are broadly seen in the simulated graphene. This is due to the ultra short time scale of the MD simulation in comparison with that of real CVD experiments, i.e., ns vs. minutes. Although the simulated structures are very different from those observed in experiments, the MD simulation reveals some insightful mechanisms of defect healing. In the simulation, various spontaneous defect healing processes are observed, which might be attributed to the accurate PES we developed for the study.[46] Figure 2a-c shows a typical healing process of a pentagon formation observed during the MD simulation. Firstly, a carbon atom is attached to the pentagon as a dangling atom and then, via the rotation of the carbon-carbon bond, a hexagon was formed consequently (figure 2b,c). Such a healing procedure occurs in the time scale of only ~ 19 ps. The potential energies for intermediate configurations of (a), (b) and (c), are shown in fig. 2d..This kind of healing has been proposed in a previous theoretical studies for carbon nanotube growth.[55] Another healing route of the pentagon is presented in Figure 2d-h, in which three carbon atoms are attached to the pentagon one by one with a carbon chain formed finally (figure 2e-g). Meanwhile, a dissolved carbon atom (in red color) embed in the subsurface (figure 2e) diffuses to the surface (figure 2f,g) and forms a hexagon by incorporating itself between a carbon-carbon bond of the pentagon. Different from the first mechanism, such a defect healing takes ~ 1.6 ns, because of the relatively complicated process and the diffusion of the red carbon atom from the subsurface. Due to such a large span of the MD time, the carbon atoms of the system are not conservative with with a energy profile the potential energies for the intemidiate processes shown in figure S2.

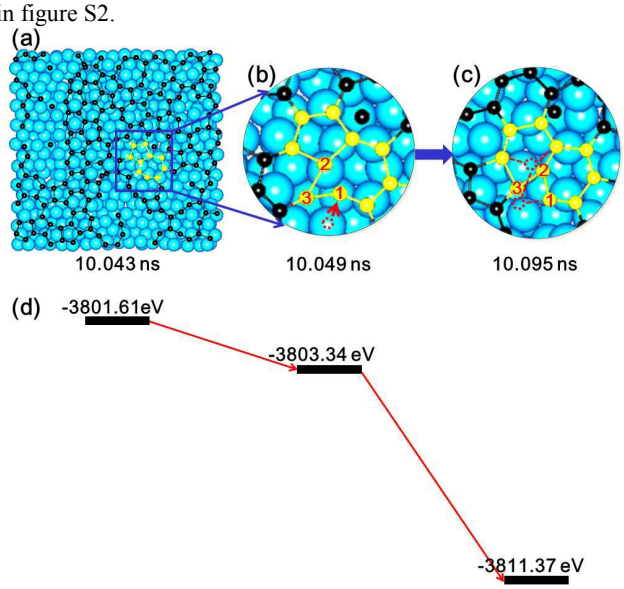

Fig. 3 The healing process of a pentagon-heptagon pair. (a)-(b) The atom C1 diffuses towards the inward of the heptagon. The red dashed circle in (b) indicates the original position of the C1 carbon atom. The red arrow in (b) indicates the diffusing direction of the C1 atom. (c) Two hexagons are formed by the clockwise rotation (~ 35°) of the carbon-carbon bond between C2 and C3. The red dashed circles indicate the original positions of C2 and C3. The red dashed lines indicate the original carbon bonds for the sake of guiding the eyes. (d) The potential energies of configurations (a),(b) and (c).

In addition to the healing of pentagon, a pentagon-heptagon pair (5|7), as shown in figure 3a, can also be healed. As displayed in figure 3b, the atom C1 diffuses to the pentagon and attacks C2, and consequently a carbon-carbon bond between C2 and C3 is rotated by ~ 35°, and then two neighboring hexagons (6|6) are formed (figure 3c). Such a small angle carbon-carbon bond rotation is equivalent to the rotation of a "shoulder bond" as proposed in the previous study.[55]

3.3 The effect of carbon deposition rate (CDR) on the quality

of the graphene

In CVD experiments, single layer graphene with higher quality are usually synthesized with lower carbon flow rate (CFR).[56] A low CFR normally leads to a low carbon deposition rate (CDR) and thus longer time for defect annealing during growth.[31, 57] Altering CDR results in same effect of turning of the CFR in experiments. Figure 4 shows the final configurations of the simulated graphene with the CDR of 20 (a) and 40 (b) ps/atom, respectively. The former shows a graphene layer with more topological defects than the latter (Figure. 4c vs. 4d) and, moreover, with many carbon atoms attached to the graphene surface, sp^3 hybridized carbons, which distort the graphene lattice severely, are observed. During the later simulation, however, a high quality graphene with less topological defects and sp^3 carbon atoms are formed due to longer annealing time during the MD simulation.

Figure 4c and d show the statistics of pentagons, hexagons, heptagons, and octagons as the function of the MD simulation time for the fast and slow CDRs, respectively. In figure 4c, there is a larger number gap between hexagons and the non-six member rings (SMRs), including pentagons, heptagons and octagons. Furthermore, the number of heptagons in figure 4d shows a platform with even a minor decrease after 10 ns and the number of pentagons in figure 4d displays a dramatic decrease after 14 ns. To be convincing, we plot the percentages of hexagons among the four carbon rings (pentagon, hexagon, heptagon, and octagon) during the final 1.5 ns (Figure 6a). Obviously, the larger the percentage of the hexagon is, the higher the graphene quality. Thus, we can conclude that the defects can be annealed more sufficiently with slow CDR, which agrees well with the previous study.[57]

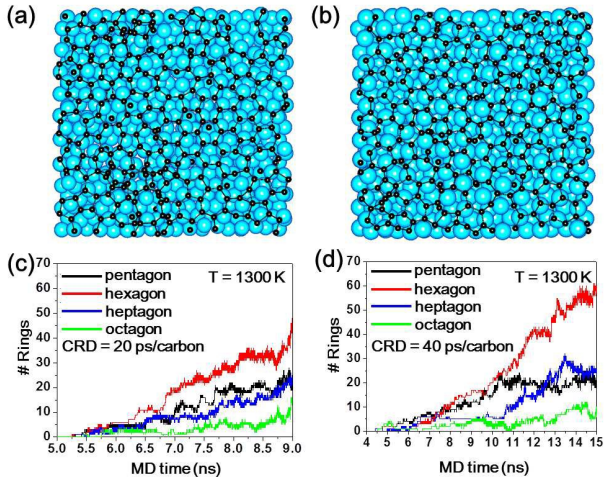

Fig. 4 The final configurations of the graphene on Ni surface simulated with CDR = 20 (a) and 40 (b) ps/carbon, respectively. (c) and (d) present the numbers of pentagons, hexagon, heptagons and octagons as the function of the MD times for CDR =20 and 40 ps/carbon, respectively.

3.4 The effect of the temperature on the graphene quality

Temperature is also a significant factor for the quality of the graphene. Previous theoretical studies show that the energy barriers for carbon diffusion, carbon precipitation, carbon incorporation, and defects healing are ~1.0, 0.5, 2.0 and 2.5 (eV), respectivley, for the nickel substrate.[58, 59] According to the rate theory R ~ exp(Eb/kT), where Eb is the energy barrier, k and T are Boltzmann constant and temperature, respectively, sufficient high temperature can provide higher kinetic energies to assist carbon atoms to overcome these barriers. However, very high temperature can destroy the nickel surface or even the graphene lattice. To study the temperature effect on the formation of graphene on Ni surface, we performed the simulations under temperature of 900 K, 1100 K, and 1300 K, respectively, with the same CDR = 40 ps/carbon.

Figure 5a shows that under lower temperature, such as 900 K, many defects are produced due to the insufficient activation of the thermal energy. With the increase of the temperature, the defects can be largely reduced (figure 5b-c). Obviously, the quality of graphene lattice grown at the temperature of 1300 K is the best compared with the other two temperatures. To confirm this, again, the statistics of pentagons, hexagons, heptagons, and octagons as the function of MD simulation times are shown in figure 5d-f. For the temperature of 900 K, the number of hexagons fails to exceed any of non-SMRs. When the temperature is increased to 1100 K, however, the number of hexagons start to exceed non-SMRs (figure 5e), which means more defects are annealed by the increased temperature. Further increase of the temperature can enlarge the gap of the number between hexagons and non-SMRs (figure 5f). Figure 6b shows the percentages of the hexagons from 9 ns to 15 ns in 900 K, 1100K and 1300 K, respectively. Since the time of the carbon network formation in the three temperatures is different, we compare the percentage of the hexagons after 9 ns, when the carbon network has been formed for each temperature. The percentage of hexagons in 1300 K can reach 50%, while only ~ 30% in 900 K. Therefore, higher temperature around 1300 K can indeed enhance the quality of the formed graphene on nickel surface. Two previous MD simulations show the optimum temperatures are 1000 K and 1100 K,[36, 37] respectively, whereas the temperature for our simulation can be 200 K higher but with better quality of the graphene. The reason can be attributed to the slow CDR (40 ps/carbon) and large time scale (15 ns) achieved during the simulation. We also note that the PES in our current study is well developed against DFT calculations.[46] Thus, higher quality of the graphene can be achieve during the CVD synthesis on Ni substrate if the carbon flow rate is well controlled (low enough) with enough high temperature, such as 1300 K, may enhance the quality of the grapehne.

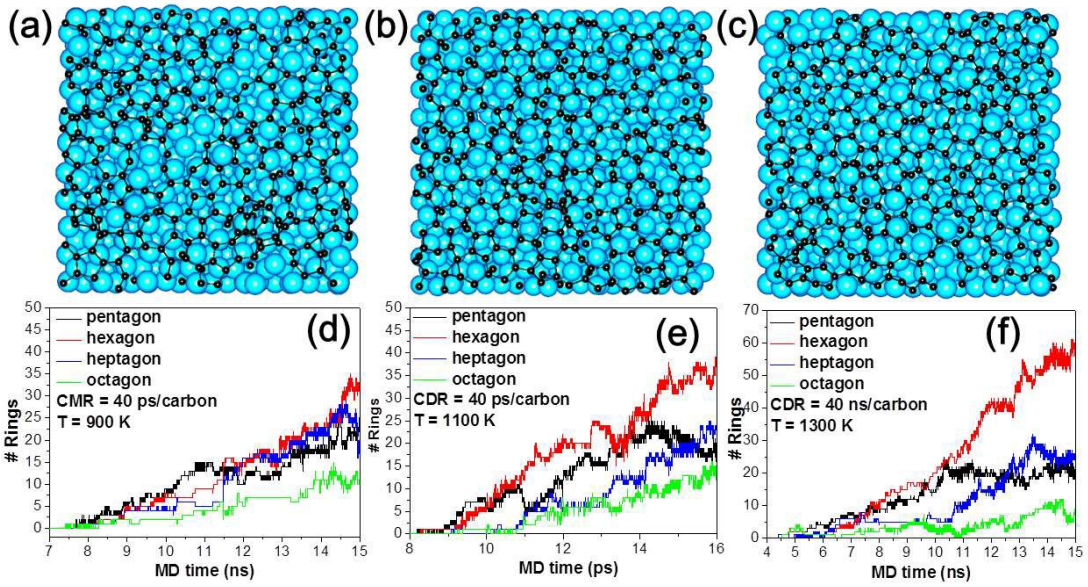

Fig. 5 (a) Graphene grown in different temperatures. (b-d) The numbers of pentagons, hexagon, heptagons and octagons as the functions of theMD timesfor T = 900 K, 1000 K, 1100 K and 1300 K, respectively.

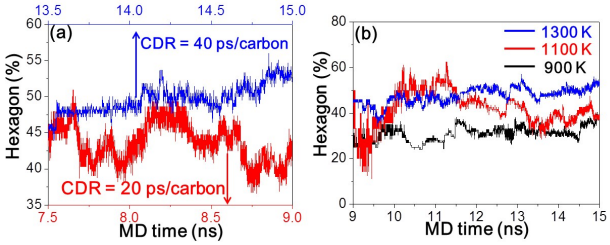

Fig. 6 (a) The percentages of hexagons among the carbon rings during the final 1.5 ns for CDR = 20 ps/carbon and CDR = 40 ps/carbon at 1300 K, respectively. (b) The percentages of the hexagons among the carbon rings from 9ns to 15 ns in 900 K, 1100 K and 1300 K with CDR = 40 ps/carbon, respectively.

4. CONCLUSIONS

In summary, classical molecular dynamics simulations are performed to study the growth mechanism of the single layer graphene on Ni(111) surface. The atomistic details from the polygon nucleation to the graphene formation show that the carbon dimers, trimmers, and chains can be formed before the nucleation of the carbon polygons. By analyzing the carbon and nickel atoms distribution along the direction normal the nickel surface, we reveal the phenomenon of the carbon dissoluti before the nucleation and carbon precipitation from the subsurface after the nucleation. The defects of pentagon and pentagon|heptagon pair can be healed at high temperature via the carbon-carbon bond rotation or the carbon incorporation with the assistance of the catalyst particle and the thermal energetic motion. Thus, our simulations demonstrate that slower CDR (sufficient annealing time) and higher temperature can improve the quality of the graphene during the CVD growth on the nickel substrate.

Acknowledgements

Z. W. Xu, G. W. Liu and G. J. Qiao acknowledge the support of NSFC grants (11404144, 51572112) and the Research Funds in Jiangsu University (14JDG120). T. Y. Yan acknowledge the support of NSFC grants (21373118).

Notes and References

[a]*School of Materials Science & Engineering, Jiangsu University, Zhenjiang 212013, Peoples Republic of China*
[b]*Institute of New Energy Material Chemistry, Collaborative Innovation Center of Chemical Science and Engineering (Tianjin), Nankai University, Tianjin 300071, Peoples Republic of China*
[c]*Institute of Textiles and Clothing, Hong Kong Polytechnic University, Hung Hom, 999077, Hong Kong, E-mail: tcfding@inet.polyu.edu.hk*

1 K.S. Novoselov, A.K. Geim, S.V. Morozov, D. Jiang, Y. Zhang, S.V. Dubonos, I.V. Grigorieva, A.A. Firsov, Science, **2004**, 306, 666-669.
2 D.A. Dikin, S. Stankovich, E.J. Zimney, R.D. Piner, G.H.B. Dommett, G. Evmenenko, S.T. Nguyen, R.S. Ruoff, Nature, **2007**, 448, 457-460.
3 T. Ohta, A. Bostwick, T. Seyller, K. Horn, E. Rotenberg, Science, **2006**, 313, 951-954.
4 S. Nie, N.C. Bartelt, J.M. Wofford, O.D. Dubon, K.F. McCarty, K. Thürmer, Phys. Rev. B, **2012**, 85, 205406.
5 T. Niu, M. Zhou, J. Zhang, Y. Feng, W. Chen, J. Am. Chem. Soc., **2013**, 135, 8409-8414.
6 J.D. Wood, S.W. Schmucker, A.S. Lyons, E. Pop, J.W. Lyding, Nano Lett., **2011**, 11, 4547-4554.
7 Y. Zhang, L. Gomez, F.N. Ishikawa, A. Madaria, K. Ryu, C.A. Wang, A. Badmaev, C.W. Zhou, J. Phys. Chem. Lett., **2010**, 1, 3101-3107.
8 A. Varykhalov, O. Rader, Phys. Rev. B, **2009**, 80, 035437.
9 D. Eom, D. Prezzi, K.T. Rim, H. Zhou, M. Lefenfeld, S. Xiao, C. Nuckolls, M.S. Hybertsen, T.F. Heinz, G.W. Flynn, Nano Lett., **2009**, 9, 2844-2848.

10 N.A. Vinogradov, A.A. Zakharov, V. Kocevski, J. Rusz, K.A. Simonov, O. Eriksson, A. Mikkelsen, E. Lundgren, A.S. Vinogradov, N. Martensson, A.B. Preobrajenski, Phys. Rev. Lett., **2012**, 109, 5.
11 L. Gao, W. Ren, H. Xu, L. Jin, Z. Wang, T. Ma, L.-P. Ma, Z. Zhang, Q. Fu, L.-M. Peng, X. Bao, H.-M. Cheng, Nat. Commun., **2012**, 3, 699.
12 D.L. Ma, M.X. Liu, T. Gao, C. Li, J.Y. Sun, Y.F. Nie, Q.Q. Ji, Y. Zhang, X.J. Song, Y.F. Zhang, Z.F. Liu, Small, **2014**, 10, 4003-4011.
13 E. Loginova, N.C. Bartelt, P.J. Feibelman, K.F. McCarty, New J. Phys., **2009**, 11, 20.
14 H. Zhang, Q. Fu, Y. Cui, D.L. Tan, X.H. Bao, J. Phys. Chem. C, **2009**, 113, 8296-8301.
15 B. Wang, M. Caffio, C. Bromley, H. Fruchtl, R. Schaub, ACS Nano, **2010**, 4, 5773-5782.
16 B.Y. Dai, L. Fu, Z.Y. Zou, M. Wang, H.T. Xu, S. Wang, Z.F. Liu, Nat. Commun., **2011**, 2, 6.
17 S.S. Chen, W.W. Cai, R.D. Piner, J.W. Suk, Y.P. Wu, Y.J. Ren, J.Y. Kang, R.S. Ruoff, Nano Lett., **2011**, 11, 3519-3525.
18 Y.P. Wu, H. Chou, H.X. Ji, Q.Z. Wu, S.S. Chen, W. Jiang, Y.F. Hao, J.Y. Kang, Y.J. Ren, R.D. Piner, R.S. Ruoff, ACS Nano, **2012**, 6, 7731-7738.
19 X.S. Li, W.W. Cai, J.H. An, S. Kim, J. Nah, D.X. Yang, R. Piner, A. Velamakanni, I. Jung, E. Tutuc, S.K. Banerjee, L. Colombo, R.S. Ruoff, Science, **2009**, 324, 1312-1314.
20 L.L. Fan, Z. Li, Z.P. Xu, K.L. Wang, J.Q. Wei, X. Li, J. Zou, D.H. Wu, H.W. Zhu, Aip Adv., **2011**, 1, 9.
21 H. Chen, W. Zhu, Z. Zhang, Phys. Rev. Lett., **2010**, 104, 186101.
22 J. Gao, J. Yip, J. Zhao, B.I. Yakobson, F. Ding, J. Am. Chem. Soc., **2011**, 133, 5009-5015.
23 Q. Yuan, J. Gao, H. Shu, J. Zhao, X. Chen, F. Ding, J. Am. Chem. Soc., **2012**, 134, 2970-2975.
24 J.F. Gao, Q.H. Yuan, H. Hu, J.J. Zhao, F. Ding, J. Phys. Chem. C, **2011**, 115, 17695-17703.
25 J. Gao, F. Ding, Angew. Chem. Int. Ed., **2014**, 53, 14031-14035.
26 Z. Li, P. Wu, C. Wang, X. Fan, W. Zhang, X. Zhai, C. Zeng, Z. Li, J. Yang, J. Hou, ACS Nano, **2011**, 5, 3385-3390.
27 W. Zhang, P. Wu, Z. Li, J. Yang, J. Phys. Chem. C, **2011**, 115, 17782-17787.
28 X. Zhang, Z. Xu, L. Hui, J. Xin, F. Ding, J. Phys. Chem. Lett., **2012**, 3, 2822-2827.
29 H.B. Shu, X.S. Chen, F. Ding, Chem. Sci., **2014**, 5, 4639-4645.
30 L. Wang, F. Yan, H.L.W. Chan, F. Ding, Nanoscale, **2012**, 4, 7489-7493.
31 L. Wang, X. Zhang, H.L.W. Chan, F. Yan, F. Ding, J. Am. Chem. Soc., **2013**, 135, 4476-4482.
32 J. Gao, J. Zhao, F. Ding, J. Am. Chem. Soc., **2012**, 134, 6204-6209.
33 H. Shu, X. Chen, X. Tao, F. Ding, ACS Nano, **2012**, 6, 3243-3250.
34 V.I. Artyukhov, Y. Liu, B.I. Yakobson, Proc. Nat. Acad. Sci., **2012**, 109, 15136-15140.
35 J.A. Elliott, Y. Shibuta, H. Amara, C. Bichara, E.C. Neyts, Nanoscale, **2013**, 5, 6662-6676.
36 L. Meng, Q. Sun, J. Wang, F. Ding, J. Phys. Chem. C, **2012**, 116, 6097-6102.
37 E.C. Neyts, A.C.T. van Duin, A. Bogaerts, Nanoscale, **2013**, 5, 7250-7255.
38 R. Rasuli, K. Mostafavi, J. Davoodi, Journal of Applied Physics, **2014**, 115, 024311.
39 H. Amara, C. Bichara, F. Ducastelle, Phys. Rev. B, **2006**, 73, 113404.
40 H. Amara, J.M. Roussel, C. Bichara, J.P. Gaspard, F. Ducastelle, Phys. Rev. B, **2009**, 79, 014109.
41 S. Karoui, H. Amara, C. Bichara, F. Ducastelle, ACS Nano, **2010**, 4, 6114-6120.
42 H.-B. Li, A.J. Page, Y. Wang, S. Irle, K. Morokuma, Chem. Commun., **2012**, 48, 7937-7939.
43 Y. Wang, A.J. Page, Y. Nishimoto, H.-J. Qian, K. Morokuma, S. Irle, J. Am. Chem. Soc., **2011**, 133, 18837-18842.
44 A.J. Page, Y. Wang, H.-B. Li, S. Irle, K. Morokuma, J. Phys. Chem. C, **2013**, 117, 14858-14864.
45 V.O. Özçelik, S. Cahangirov, S. Ciraci, Phys. Rev. B, **2012**, 85, 235456.
46 Z. Xu, T. Yan, F. Ding, Chem. Sci., **2015**, 6, 4704-4711.
47 D.W. Brenner, O.A. Shenderova, J.A. Harrison, S.J. Stuart, B. Ni, S.B. Sinnott, J. Phys.: Condens. Matter, **2002**, 14, 783-802.
48 M.A. Karolewski, Radiat Eff. Defects Solids, **2001**, 153, 239-255.
49 Y. Yamaguchi, S. Maruyama, The European Physical Journal D - Atomic, Molecular, Optical and Plasma Physics, **1999**, 9, 385-388.
50 F. Ding, K. Bolton, A. Rosén, Computational Materials Science, **2006**, 35, 243-246.
51 A. Martinez-Limia, J. Zhao, P.B. Balbuena, Journal of Molecular Modeling, **2007**, 13, 595-600.
52 H.J.C. Berendsen, J.P.M. Postma, W.F. van Gunsteren, A. DiNola, J.R. Haak, J. Chem. Phys., **1984**, 81, 3684-3690.
53 M. Jiao, H. Qian, A. Page, K. Li, Y. Wang, Z. Wu, S. Irle, K. Morokuma, J. Phys. Chem. C, **2014**, 118, 11078-11084.
54 M. Jiao, K. Li, Y. Wang, Z. Wu, J. Phys. Chem. C, **2015**, 119, 12643-12650.
55 Q. Yuan, Z. Xu, B.I. Yakobson, F. Ding, Phys. Rev. Lett., **2012**, 108, 245505.
56 A. Reina, X. Jia, J. Ho, D. Nezich, H. Son, V. Bulovic, M.S. Dresselhaus, J. Kong, Nano Lett., **2008**, 9, 30-35.
57 A.J. Page, Y. Ohta, Y. Okamoto, S. Irle, K. Morokuma, J. Phys. Chem. C, **2009**, 113, 20198-20207.
58 Q. Yuan, H. Hu, F. Ding, Phys. Rev. Lett., **2011**, 107, 156101.
59 D. Cheng, G. Barcaro, J.-C. Charlier, M. Hou, A. Fortunelli, J. Phys. Chem. C, **2011**, 115, 10537-10543.